

Compaction bands induced by borehole drilling

R. Katsman · E. Aharonov · B. C. Haimson

Received: 13 June 2008 / Accepted: 17 March 2009 / Published online: 24 April 2009
© Springer-Verlag 2009

Abstract Drilling experiments in rock blocks subjected to pre-existing true triaxial far-field stresses simulating real in situ conditions often result in localized failure around the created borehole, which brings about the formation of borehole breakouts. In weakly bonded quartz-rich porous sandstones breakouts take the form of narrow tabular (slot-like) openings extending along a plane perpendicular to the maximum applied-stress direction. Scanning electron microscopes images of failed boreholes strongly suggest that these breakouts are compaction bands that have been emptied to different extents. The bands form as a result of the stress concentration accompanying the creation of the borehole. The evacuation of the compaction bands is brought about by the circulating drilling fluid flushing out debonded and often fragmented grains from within these bands (Haimson and co-workers, 2003–2007). The objective of this paper is to predict the conditions under which compaction bands are formed around boreholes. To this end, a new analytical model is formulated that enables prediction of the stress field around emptied and filled compaction bands, the various factors affecting the breakouts lengths, and their final length. Good agreement of the developed analytical model with experimental results obtained by Haimson and co-workers (Haimson and Klaetsch in Rock physics and geomechanics in the study of

reservoirs and repositories, vol 284, pp 89–105, 2007; Haimson and Kovachich in Eng Geol 69:219–231, 2003; Klaetsch and Haimson in Mining and tunneling innovation and opportunity, University of Toronto press, pp 1365–1371, 2002; Sheets and Haimson in Proceedings, paper ARMA/NARMS 04-484, 2004) is demonstrated. The presented study is of practical relevance: boreholes are often drilled deep into weak porous sandstone formations for the purpose of extracting oil and gas, and the question of borehole stability is crucial. In addition, borehole breakouts are often used to estimate the state of stress in the Earth's crust, and our new formulation will help improve these estimates.

Keywords Borehole · Borehole breakout · Borehole drilling · Compaction band · Rock mechanics

1 Introduction

Boreholes drilled into the Earth's crust for facilitating the extraction of water, oil, natural gas, geothermal steam, or for enabling geophysical observations, can reach depths of several kilometers, where in situ stresses are high and rock formations can be rather weak. During or immediately after drilling, boreholes often develop 'breakouts' that form as a consequence of stress-induced rock failure. Breakouts initiate at the borehole wall, at points subjected to the highest compressive stress concentration resulting from the pre-existing far-field in situ stress. Field observations and laboratory test results have supported theoretical findings that in vertical boreholes breakouts are aligned with the direction of the minimum horizontal in situ stress, σ_3 along which the maximum tangential compressive stress prevails [8, 12]. To date, numerous vertical boreholes (in particular

R. Katsman (✉) · E. Aharonov
Faculty of Science, The Institute of Earth Sciences,
The Hebrew University of Jerusalem, Givat Ram,
91904 Jerusalem, Israel
e-mail: reginak@savion.huji.ac.il

B. C. Haimson
Department of Materials Science and the Geological
Engineering Program, University of Wisconsin-Madison,
1509 University Ave., Madison, WI 53706-1595, USA

oil-field wellbores) have been logged and their breakout orientations used to estimate regional principal in situ stress directions, rendering them a major contributor to the World Stress Map [29]. In addition, it has been shown that definite correlations exist between borehole breakout dimensions and in situ stress magnitudes in laboratory rock samples [15, 33]. Vernik and Zoback [37], Brudy et al. [3], and Haimson and Chang [11] successfully utilized logged breakout spans and known rock criteria of failure to estimate the maximum horizontal in situ stress, σ_1 , in the deep scientific holes of Cajun Pass, California and KTB, Germany.

A comprehensive analysis of different theoretical, numerical, and experimental approaches analyzing borehole instability leading to breakouts in rocks is provided by Germanovich and Dyskin [7]. Haimson [10] reviews several distinct grain-scale failure mechanisms that bring about borehole breakouts based on microscopic observations of specimens tested in the laboratory. He distinguishes between two major types of breakouts. In granite, limestone, and well-cemented arkosic sandstone, critical in situ stresses lead to the development of intra- and transgranular densely-spaced dilatant microcracks behind the borehole wall along the σ_3 springline. The microcracks create thin rock flakes that are too slender to support the prevailing compressive tangential stress. They buckle and fall out in sequential order giving rise to V-shaped (dog eared) breakouts.

However, in medium to high-porosity (10–30%) quartz-rich sandstones, which typically have weakly suture-bonded grains, borehole failure takes the shape of narrow slot-like breakouts extending along the direction of σ_3 . Experimental evidence suggests that the high concentration of compressive stress along the σ_3 springline brings about the debonding of a narrow band of grains and its subsequent compaction, often accompanied by grain splitting and shattering [13, 14, 16, 31]. This compacted zone is remarkably similar to the recently recognized geological structure named compaction band or ‘CB’ [26]. The loosened grains and fragments are sequentially removed to various degrees from the CB by the circulating drilling fluid, creating the slot-shaped breakout. Hence, these breakouts can be considered emptied CBs.

Haimson and Kovacich [14] and Sheets and Haimson [31] investigated the effect of different drilling parameters on the occurrence of slot-shaped breakouts in high-porosity, quartz-rich Berea and Mansfield sandstones. One of their observations was that breakout length is directly correlatable to the magnitude of σ_1 under otherwise identical far-field stress and drilling conditions. Similarly, higher flow-rates of the circulating drilling fluid improve the efficiency of the CB loosened grain removal, thus extending breakout length. Hence, breakout length and

circulating fluid flow rate are also correlatable. The two extreme cases, one of totally emptied CB, and the other of practically un-emptied CB, are characterized by disparate stress fields [22, 23]. Specifically, the stresses at the tips of completely emptied and those of un-emptied CBs are different. Therefore the character of their propagation and thus their final length is also dissimilar.

Compaction bands (also as associated with slot-like breakouts) in medium to high-porosity quartz-rich sandstones were studied theoretically by Katsman and coworkers [20–23]. Different compaction patterns, i.e., localized, diffuse, and distributed compaction were modeled numerically, successfully reproducing results of Klein et al. [25], Olsson [28], Issen and Rudnicki [17, 18], and Baud et al. [1]. Katsman et al. [20] showed that the different patterns were controlled by the degree of heterogeneity in the host rock, while the nucleation of compaction fronts was driven by the existence of a stiff experimental end cap and the resulting spatial contrast in elastic properties.

The nucleation of CBs near defects of different nature, like cracks, notches [34–36], and previously created CBs was also modeled numerically in [21], and results were found to be in agreement with experimental observations. The theoretical and numerical analysis showed that the compaction process is initiated by compressive stress concentrations. Such stress concentrations exist in the vicinity of defects. In particular, CBs emanate from highly stressed tips of cracks or notches. Katsman et al. [22] proposed to characterize CBs as a localized volume reduction (LVR) feature resulting from the localized plastic strain caused by irreversible grain crushing and porosity reduction produced by mechanical compaction, and numerically calculated the stress in the vicinity of such an LVR defect. An analytical solution, based on the Eshelby [5] transformation problem formulation, was developed by Katsman et al. [23] and found to be in agreement with the earlier developed numerical model [22]. It was found that the source of the stress enhancement at the CB tips is the geometrical incompatibility of the created CB with the surrounding matrix (rather than stiffness loss as in cracks).

This paper describes a new analytical model (built upon our previous works [22, 23]) that was developed in order to study the stress field around emptied and filled CBs emanating from boreholes, and determine factors affecting final breakout lengths. It is shown that rapid growth of empty defects, like cracks or emptied CBs, is the result of the inability of these defects to carry the applied load under either compression or extension. This enables the stress at their tips to grow rapidly as the defects elongate. In contrast, filled volume reduction defects, like un-emptied CBs, do transmit the applied load and are characterized by constant tip stress (similar to the one developed by edge

dislocations), and thus there is no reason for rapid defect lengthening. Good agreement of the developed analytical model with the results of the experiments of Haimson and co-workers [13, 14, 24, 31] is clearly demonstrated in the following. We propose that our new model enables correlation between the length of CBs, the loading conditions, and the extent of CB emptying.

2 Summary of experimental work

2.1 Experimental setup and procedure

The laboratory drilling experiments carried out at the University of Wisconsin have been described in detail by Haimson [9]. They involve drilling central vertical holes (normally 20 mm in diameter) in rock blocks, typically of size 150 × 150 × 230 mm. The blocks are drilled through while subjected to preset true triaxial far-field stresses generated by compressive loads applied to their surfaces, such that the vertical (σ_2), and the maximum and minimum horizontal principal stresses (σ_1 and σ_3) are all unequal and of magnitudes replicating typical field conditions. Drilling fluid (usually tap water) is circulated at a prescribed flow rate through the borehole as it is created. This fluid evacuates the chips and debris created by the drilling operation. When breakouts are induced during drilling, the circulating fluid flushes out debonded grains and fragments from within the breakout. At the conclusion of drilling the borehole is immediately filled with epoxy to preserve borehole wall conditions. Cross sections of the tested blocks are then studied to establish whether breakouts were formed, and if so, to determine their geometry and orientation. Optical and scanning electron microscopes (SEM) are used to observe the grain-scale mechanism leading to breakout formation.

2.2 Rock types and experimental results

In this paper, we concentrate on two series of tests, one in Berea sandstone (abbreviated here as BS), in particular the high porosity variety, and one in Mansfield sandstone (abbreviated here as MS). Both rocks have porosities in excess of 20%, are quartz-rich, with grains that are predominantly bonded by weak suturing and by little, if any, cementing material. Table 1 presents some physical and mechanical properties of these rocks as determined in our laboratory.

Detailed results of the drilling experiments have been published before [14, 31]. Generally, breakouts in both rocks were slot-shaped and only several grain diameters wide, and extended along a plane perpendicular to the maximum stress σ_1 (Figs. 1, 2). In this paper, we focus

Table 1 Physical and mechanical properties of Berea and Mansfield sandstones

Properties	Berea sandstone (BS)	Mansfield sandstone (MS)
Mineral composition	Quartz 80%, feldspar 12%	Quartz 90%, mica 7%
Primary grain bonding	Sutured grain contacts	Sutured grain contacts
Uniaxial compressive strength	24.6 MPa	19.3 MPa
Brazilian tensile strength	1.7 MPa	1.1 MPa
Rock cohesion	11.0 MPa	8.4 MPa
Internal friction angle	33°	41°
Porosity 3D	25%	27%
Porosity 2D	28%	22%
Porosity 2D after comp.	12.7%	17.9%
Poisson ratio	0.25	0.25
Band's half-width after compaction, h	1.65 mm	1.15 mm
Young's modulus	9.24 GPa	9.6 GPa
Grain diameter	0.5 mm	0.24 mm
Borehole radius	11.5 mm	11.5 mm
ΔP excess fluid pressure	0.4 MPa	0.4 MPa

only on some of the experimental results in these two rocks, those concerning the formation of breakouts that can be viewed as un-emptied or filled CBs (Fig. 1a), and at the other extreme slot-like breakouts that are practically fully emptied CBs (Fig. 2a). These two kinds of defects are reviewed in the following section.

3 Breakout geometry

Two general end-member types of experimentally observed breakouts (out of the three described below) are analyzed analytically:

1. *Un-emptied CB emanating from a borehole* (Fig. 1) This type of breakout is created under conditions of very low fluid flow rate (0.01 L/s, as in [14]) at the locations given in Fig. 1. The low flow rate is insufficient to evacuate the compacted and loosened grains from the created CB into the borehole. Although, typically, there is going to be a trace of breakout even when the drilling circulating fluid is ineffective (Fig. 1a), sufficiently low flow rate can be modeled as incapable of evacuating the compacted and loosened grains from the created CB into the borehole. Such a breakout can also be created by using heavy drilling mud instead of water, as in Sheets and Haimson [31], Figs. 11c, 12. In this case, the thin

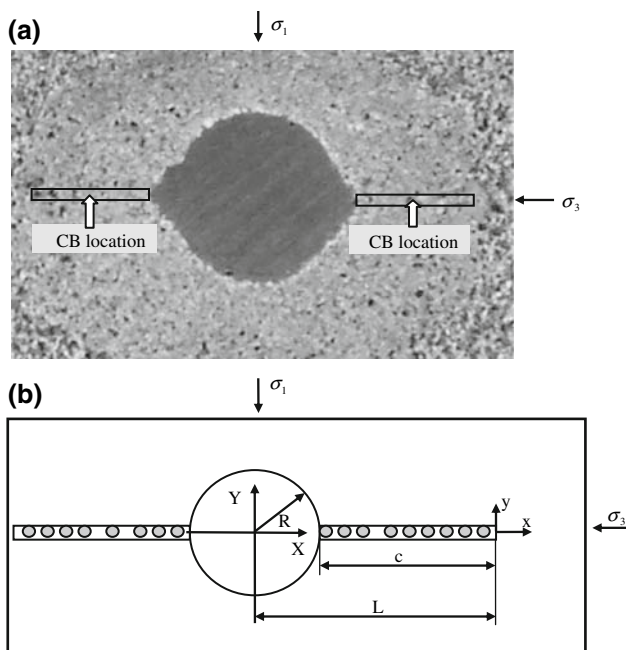


Fig. 1 Un-emptied compaction band (CB) emanating from a borehole **a** in a macro photograph of a cross section of tested Mansfield sandstone showing just a hint of a breakout, signifying an un-emptied CB. The CB is not seen as it requires high magnification photomicrography (see for example Haimson and Klaetsch [13]); **b** CBs as simulated by model. R is the borehole radius, L the length from the borehole center to the breakout tip, c the breakout length, and σ_1 and σ_3 are the principal stresses applied to the tested specimen. The (X, Y) coordinate origin is positioned at the borehole center. The (x, y) coordinate origin is positioned at the compaction band tip

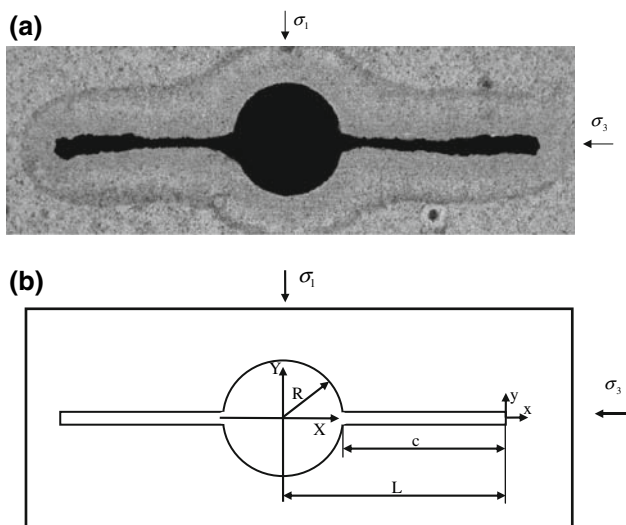


Fig. 2 Emptied compaction bands emanating from a borehole **a** as seen in cross section of tested Mansfield sandstone and **b** as simulated by model. R is the borehole radius, L the length from the borehole center to the breakout tip, c the breakout length, and σ_1 and σ_3 are the principal stresses applied to the tested specimen. The (X, Y) coordinate origin is positioned at the borehole center. The (x, y) coordinate origin is positioned at the compaction band tip

layer of drilling mud, referred to as “mud cake”, creates a nearly impermeable lining that prevents the removal and evacuation of compacted and loosened grains from the CB into the borehole ([31], Fig. 14a). Thus, under these conditions, the CBs remain filled with compacted and loosened grains.

2. Emptied CB emanating from a borehole (Fig. 2). Under conditions of high flow rate (such as 0.06 L/s, as in [14], Figs. 8, 9c), the circulating fluid can be modeled as immediately evacuating all the compacted and loosened grains created within the CB, thus creating a slot-like empty CB emanating from the borehole (Fig. 2a). This is, of course, an idealization since commonly we observe some loosened and cracked grains ahead of the breakout tip even in such situations (example in Fig. 14b, [31]), but the length of this zone as compared to that of the created breakout is usually negligible.
3. Partially emptied CB emanating from a borehole. At intermediate flow rates only a fraction of the compacted and loosened grains are removed from the created CB. As a result, a part of the breakout adjacent to the borehole is emptied; however, the rest of the breakout (located near the tip) remains filled with compacted and loosened grains (see Fig. 22 in [10]). This transient case is not considered in the current study; it will be studied in a separate manuscript which is currently in preparation.

4 Model

This section describes the analytical models created to predict the length of both emptied and un-emptied CBs under different loading conditions.

4.1 Stresses

The variable that determines whether CBs arrest or whether they progressively lengthen is the level of enhanced stresses at their tip. The enhanced stress at the tip arises from a combination of (1) the stress induced by the defect itself (the un-emptied or emptied CB) and (2) the stress induced by the presence of a hole (the borehole), which may be located farther away from the defect tip.

We consider a borehole drilled vertically into the earth’s crust, parallel to the principal stress σ_2 . The other two principal stresses (σ_1, σ_3 , Figs. 1, 2) are horizontal and are specified as loading boundary conditions at infinity. Under these conditions the strain in the vertical Z direction is constant, $\epsilon_{zz} = \partial w / \partial z = \epsilon = \text{const}$, where the vertical displacement w is independent of X and Y , the horizontal axes. In this case, σ_{xx} and σ_{yy} depend only on X and Y , as under

either plane strain or generalized plane stress conditions ([19], Section 5.3, case vii). Note that plane strain conditions are a sub-case of constant strain conditions under the assumption that $\varepsilon = 0$.

In what follows we analyze the 3D stress field for two cases (1) un-emptied CB emanating from a borehole, and case (2) emptied CB emanating from a borehole.

4.1.1 Un-emptied CB emanating from a borehole

The stress at the vicinity of an un-emptied CB is a linear combination of (1) the stress induced by a borehole under compression (considered as a “background” stress) and (2) the stress induced by the adjacent CB (Fig. 1).

1. Stress induced by a borehole under compression:

The state of stress in the X – Y plane in the vicinity of such a vertical borehole, assuming that the borehole fluid does not communicate with the pore fluid in the rock, and that the pore pressure in the rock is constant, can be expressed by the well known Kirsch equations for a hole in an infinite plate. These equations for stress around a borehole were modified by Fairhurst [6] for the case of plane strain in 3D, and updated to include the effect of pore fluid pressures. These equations are formulated in cylindrical coordinates and presented in [10].

Equation 1 in [10] demonstrates that stresses on the perimeter of a hole, placed under differential compression, reach a maximum compressive value in the X – Y plane on the points that are in an angle $\theta = \pm\pi/2$, from σ_1 (see Fig. 3 in [10]), in the direction of σ_3 . Therefore, based on both the above statement and the experimental results [14, 31], we assume from hereon that compaction will propagate along the σ_3 direction, and define the direction of σ_3 as the X axis (see Fig. 1). We restrict our analysis to stress evolution along this line, and formulate the equations in Cartesian coordinates.

The horizontal stress components, σ_{xx}^b and σ_{yy}^b , induced by a borehole filled with a fluid with an excess fluid pressure ΔP , placed under remote compression, are equal to those developed for either generalized plane stress or plane strain 2D problems [10, 19 (Section 10.4), 32]. These stress components are calculated according to Eq. 1 in Haimson [10], using $\theta = \pi/2$ (along the X axis, Fig. 1b):

$$\sigma_{xx}^b = \frac{\sigma_1 + \sigma_3}{2} \left(1 - \frac{R^2}{L^2}\right) - \frac{\sigma_1 - \sigma_3}{2} \left(1 - 4\frac{R^2}{L^2} + 3\frac{R^4}{L^4}\right) + \Delta P \frac{R^2}{L^2} \tag{1a}$$

$$\sigma_{yy}^b = \frac{\sigma_1 + \sigma_3}{2} \left(1 + \frac{R^2}{L^2}\right) + \frac{\sigma_1 - \sigma_3}{2} \left(1 + 3\frac{R^4}{L^4}\right) - \Delta P \frac{R^2}{L^2} \tag{1b}$$

where R is the borehole radius, L the length from the borehole center to the CB tip, and σ_1 and σ_3 are the horizontal principal stresses applied to the tested specimen (Fig. 1b). The (X, Y) coordinate origin is positioned at the borehole center.

Since it was experimentally observed that CBs emanating from the hole in both Berea and Mansfield sandstones had uniform thickness [15, 31], CB thickness variations are not studied in the current model and stresses are evaluated along the X axis only.

2. Stress induced by a CB

Following the theoretical and numerical study of Katsman et al. [23], the stress in the vicinity of a CB is similar to that of an edge dislocation. Edge dislocations are constructed by insertion of an “extra” plane, of width b (in the Y direction), into a lattice of atoms (Fig. 3). In a macroscopic analogy, a CB is constructed by removing a plane of width b and length $2c$, from an elastic body (Fig. 3), where $b = 2(H - h)$,

$$b = 2(H - h), \tag{2}$$

with H defined as the half-width of the CB material before it underwent compaction, and h is the CB half-width after compaction, Fig. 4, and Table 1. The plastic strain that is accommodated by the compaction process within a CB, $b/2H$, may be calculated from the porosity reduction that occurred within the CB, using Eq. 3 in Katsman and Aharonov [21]:

$$\frac{b}{2H} = \frac{\phi_{init} - \phi_{comp}}{1 - \phi_{comp}}, \tag{3}$$

The width b is thus calculated from Eqs. 2 and 3 using the CB thickness, H , and the initial and final porosities, ϕ_{init} , and ϕ_{comp} (Table 1). Having obtained b , the stress components around a CB may be calculated using the formulation outlined in Katsman et al. [23]. Since the

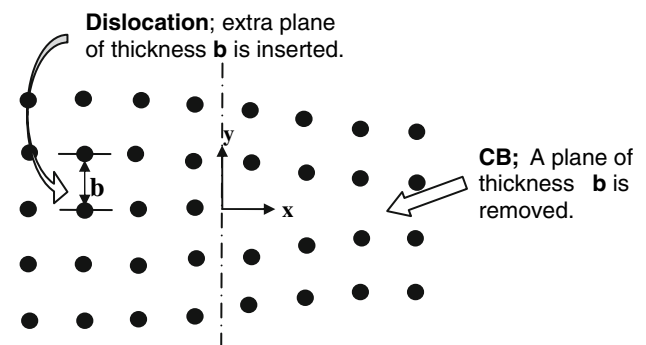


Fig. 3 Compaction band formation interpreted in terms of edge-dislocations. Edge dislocations are constructed by insertion of an “extra” half-plane, of thickness b , into an elastic body. In contrast, a compaction band is constructed by removal of a half-plane of thickness b from an elastic body

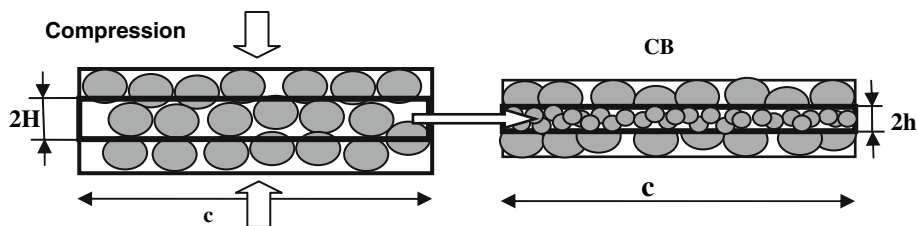


Fig. 4 Localized volume reduction during compaction band formation in a high-porosity rock. The process is characterized by vertical shortening ($2H$ before compaction, $2h$ after compaction), with no lateral shortening (c the length of the band before and after Localized volume reduction)

stresses around a CB are nearly independent of its length [23] we use the half-infinite approximation:

$$\sigma_{xx}^{CB} = -bA \frac{x(y^2 - x^2)}{(y^2 + x^2)^2}, \tag{4a}$$

$$\sigma_{yy}^{CB} = bA \frac{x(3y^2 + x^2)}{(y^2 + x^2)^2}, \tag{4b}$$

$$A \equiv \frac{\mu}{2\pi(1 - \nu)} \tag{4c}$$

Here the origin of the coordinates (x, y) is positioned at the CB tip, Figs. 1b, 2b, where x is defined as $x = X - L$.

The stresses responsible for the propagation of a CB are the ones right at the tip of a CB ($x = 0$). However, the stress analytically predicted at $x \rightarrow 0$ ($y = 0$) is singular, similar to the singularity arising at crack tips. To avoid this singularity [30] one may define the tip stress as the stress at some infinitesimal distance x_0 from the CB tip (along $Y = 0$), defined as a compactive process zone length, so that from Eqs. 4a, b:

$$\sigma_{xx}^{CB}(\text{tip}) = \sigma_{yy}^{CB}(\text{tip}) = A \frac{b}{x_0}. \tag{5}$$

The choice of x_0 is discussed in the Appendix.

3. Total stresses around an un-emptied CB emanating from the borehole

The horizontal stress components at the tip of a CB that emanates from a borehole are a linear combination of the (1) “background” compressive stress induced by the compressed borehole (Eq. 1a, 1b); (2) and the compressive stress induced by the CB itself (Eq. 5):

$$\sigma_{xx} = \sigma_{xx}^b + \sigma_{xx}^{CB} \tag{6a}$$

$$\sigma_{yy} = \sigma_{yy}^b + \sigma_{yy}^{CB} \tag{6b}$$

The vertical stress component σ_{zz} at the CB tip under the considered constant strain conditions ($\varepsilon = \text{const} \neq 0$) is a function of σ_{xx} and σ_{yy} (Eq. 6): $\sigma_{zz} = E\varepsilon + \nu(\sigma_{xx} + \sigma_{yy})$ (Eq. 22, Section 5.4, in [19]), while on the macro-scale $E\varepsilon = \sigma_2 - \nu(\sigma_1 + \sigma_3)$.

As a result, combining Eqs. (1, 5, 6), and the above basic equations from [19]

$$\sigma_{zz} = 2\nu \left[(\sigma_1 - \sigma_3) \frac{R^2}{L^2} + A \frac{b}{x_0} \right] + \sigma_2 \tag{6c}$$

4.1.2 An emptied CB emanating from a borehole

In this section, we follow the logic outlined in Sect. 4.1.1 to calculate the horizontal stress components σ_{xx} and σ_{yy} , and the vertical stress component σ_{zz} under constant strain conditions in the Z direction. Because cracks in extension and compression produce equivalent stress fields, differing in signs only (e.g., [22]), we consider empty CBs as geometrically equivalent to slot-shaped cracks under compression. Thus, the horizontal stress components σ_{xx} and σ_{yy} at the tip of a slot-like empty CB adjacent to a borehole at $Y = 0$, are equal to stresses near the tip of a 2D Mode I crack placed under either plane strain (or generalized plane stress) conditions (Fig. 2):

$$\sigma_{xx} = \sigma_{yy} = \frac{K_I}{\sqrt{2\pi x_0}}, \tag{7a}$$

where K_I is the stress-intensity factor in *Mode I* loading, and x_0 is a compactive process zone length.

For the specific configuration depicted in Fig. 2b, the stress-intensity factor is formulated in Murakami [27], Sih [32]:

$$K_I = F\sigma_1\sqrt{\pi L}, \tag{7b}$$

F is a tabulated function depending on the loading conditions, and the relation between the borehole radius and the breakout length.

Further, using Eq. 7a and Eq. 22 (Section 5.4) in [19] shown above, the vertical stress component is found to be

$$\sigma_{zz} = \sqrt{2}\nu \frac{K_I}{\sqrt{\pi x_0}} + \sigma_2 - \nu(\sigma_1 + \sigma_3) \tag{7c}$$

A comparison between Eqs. 1–6 and 7a–c demonstrates that the stress field at the tips of the emptied and un-emptied CBs is completely different.

4.2 The yield function, f

After establishing the stresses at the tips of the two types of defects, we predict how long these defects will turn out to be. When stresses at the tip of the emptied/un-emptied CB (Eqs. 1–6, or 7) attain the critical values specified by an appropriate yield criterion, compaction will propagate. Following Tembe et al. [34] and Baud et al. [2], the material yield function f is assumed to depend only on the plastic volumetric strain as the rock undergoes inelastic deformation and work hardening. f is formulated as a function of the first two stress invariants I_1 and J_2 :

$$I_1 = (\sigma_1 - P_p) + (\sigma_2 - P_p) + (\sigma_3 - P_p) \tag{8a}$$

$$J_2 = \frac{[(\sigma_1 - \sigma_2)^2 + (\sigma_2 - \sigma_3)^2 + (\sigma_3 - \sigma_1)^2]}{6 + \sigma_{12}^2 + \sigma_{23}^2 + \sigma_{13}^2} \tag{8b}$$

and is independent of the third stress invariant [2, 34].

The constitutive model considered here, and in [2, 34], adopts a yield function of the form:

$$f(\sigma_{ij}) = \frac{(I_1 - c)^2}{a^2} + \frac{J_2}{b^2} - 1 = 0 \tag{9}$$

which corresponds to an ellipse centered at $(c, 0)$ with major and minor semi axes of a and b . The parameters a , b , and c for the yield envelope of the specific rock studied here (BS and MS) are not available in the literature. Hence, these are estimated from Baud et al. [2] considering rocks closest to BS and MS in their quartz contents (these parameters for Berea and Bentheim sandstones, evaluated by [2], are presented in Table 2). Parameters a , b , and c relate to A , B , and C formulated for the Critical State Model in [2], Table 3 (Table 2 here), as $A = a/3$, $B = \sqrt{3}b$, and $C = c/3$.

Compaction propagation depends on the value of f : If $f(\sigma_{ij}) \geq 0$, localized compaction is expected to occur,

Table 2 Physical properties and Critical State Model parameters for Berea and Bentheim sandstones (taken from Baud et al. [2])

Sandstone	Porosity (%)	Grain radius (mm)	Amount of quartz (%)	a (MPa)	b (MPa)	c (MPa)
Berea	21	0.13	75	570	114	570
Bentheim	22.8	0.105	95	600	131	654

Table 3 Simulation conditions, theoretical breakout length in comparison with experimental length

Case #	Rock type	Type of breakout	σ_1 (MPa)	σ_2 (MPa)	σ_3 (MPa)	Theoretical length (mm)	Experimental length (mm)
1	BS	Non-emptied	100	50	40	15.7	13.8
2	BS	Non-emptied	90	50	40	9.2	11.5
3	MS	Non-emptied	50	40	30	3.5	3.5
4	MS	Emptied	50	40	30	Infinity	35.5

leading to CB formation; however, if $f(\sigma_{ij})$ drops below zero CB propagation is arrested [34]. As the stress field at the defect tip is responsible for the defect propagation, we assume that the yield envelope described in Eq. 9 is applicable not only for large specimens (18.4 x 38.1 mm) as in [2], but also for the smaller scale of a defect tip with dimensions of process zone length, x_0 . Further, zooming into the scale of a defect tip requires that we use the actual stress components at the tip of a defect (calculated from Eqs. 6 or 7) instead of the macroscopic principal stresses for which the yield envelope was originally formulated (Eq. 8).

The final step in calculating the CB length is seeking the point when the yield function (Eq. 9) vanishes: The intersection point of the $f(\sigma_{ij})$ curve with zero will predict the final breakout length, c (see Figs. 6, 7, 8, 9), since once $f(\sigma_{ij})$ drops below zero the CB propagation is arrested.

5 Results

This section compares predictions for CB lengths, calculated using the analytical model described in Sect. 4, with the experimental results reported by Haimson and Kovacich [14], and Sheets and Haimson [31]. The experiments revealed that the breakout length is a function of two parameters (among other factors):

1. The value of the maximum principal stress, σ_1 , for given σ_2 and σ_3 , studied here only for the case of un-emptied CBs;
2. The extent of CB emptying. Two end-members of this parameter are studied here, i.e., completely emptied CBs and un-emptied CBs. Flow rates required to produce these two extreme cases of CBs are not studied in this paper.

The effect of varying these parameters in the model is analyzed below and compared to the experimental results. Simulation conditions are presented in Table 3.

5.1 Influence of the maximum principal stress magnitude, σ_1

The length of *un-emptied* CBs (Fig. 1), created experimentally under conditions of very low flow rate (0.01 L/s, [14]),

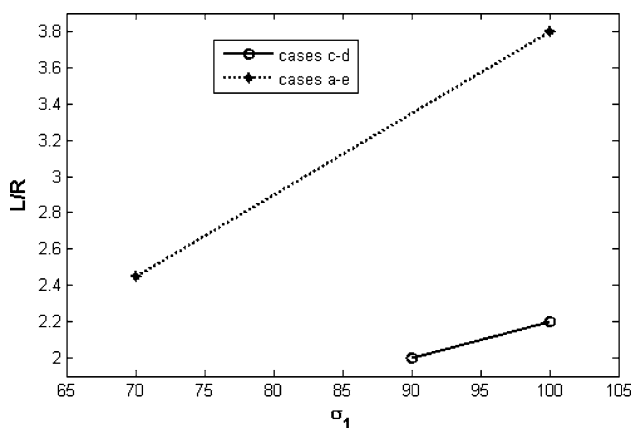


Fig. 5 Results from experiments reported in Haimson and Kovacich [14] where Berea Sandstone with a drilled borehole is compressed under various values of applied maximum principal stress σ_1 but identical values of σ_3 and σ_2 . L/R , the distance from the borehole center to the breakout tip normalized by the radius, grows with increasing σ_1 . In cases **c, d** $\sigma_2 = 50$ MPa, while in cases **a–e** $\sigma_2 = 60$ MPa. Cases **c, d** are modeled in the current paper

is compared to theoretical predictions. Experimental results for these un-emptied CBs demonstrate that increasing σ_1 leads to creation of longer CBs (Fig. 5). We use our model to predict un-emptied CB length for two different applied loads: case (1) $\sigma_1 = 100$ MPa, $\sigma_3 = 40$ MPa, and $\sigma_2 = 50$ MPa, and case (2) $\sigma_1 = 90$ MPa, $\sigma_3 = 40$ MPa, and $\sigma_2 = 50$ MPa. In both cases, Berea Sandstone (BS) is considered (Tables 1, 3). A yield function $f(\sigma_{ij})$ is calculated for Berea Sandstone [2], Table 2 here, since it is the rock closest to BS in Quartz content. For this calculation the process zone length, x_0 , was found to be ~ 8 grain diameters ($x_0 = 2.2$ mm) (see the Appendix for a detailed explanation).

Case 1, an un-emptied CB, applied load $\sigma_1 = 100$ MPa, $\sigma_3 = 40$ MPa, and $\sigma_2 = 50$ MPa (Table 2). As explained in Sect. 4.1, σ_{xx} , σ_{yy} , and σ_{zz} are calculated from Eqs. 1–6 and plotted on Fig. 6a. The solid line in Fig. 6b is the calculated yield function $f(\sigma_{ij})$ (Eq. 9) for Berea Sandstone [2]. Once $f(\sigma_{ij})$ drops below zero, CB propagation stops. The predicted breakout length (Fig. 6b) is $c = 15.7$ mm (Table 3). The experimentally measured $L/R = 2.2$ in Haimson and Kovacich [14], (their Fig. 10), yields $c = 13.8$ mm.

Case 2, an un-emptied CB, $\sigma_1 = 90$ MPa, $\sigma_3 = 40$ MPa, and $\sigma_2 = 50$ MPa (Table 3; Fig. 7a, b). The procedure we follow is identical to Case 1 (Fig. 6a, b). The theoretically predicted breakout length is $c = 9.2$ mm (Table 3). The experimentally measured $L/R = 2.0$ derived from Haimson and Kovacich [14], their Fig. 10, yields $2c = 11.5$ mm.

5.2 The extent of CB emptying

Two additional cases are modeled to study the influence of the extent of CB emptying (emptied/un-emptied) on its final

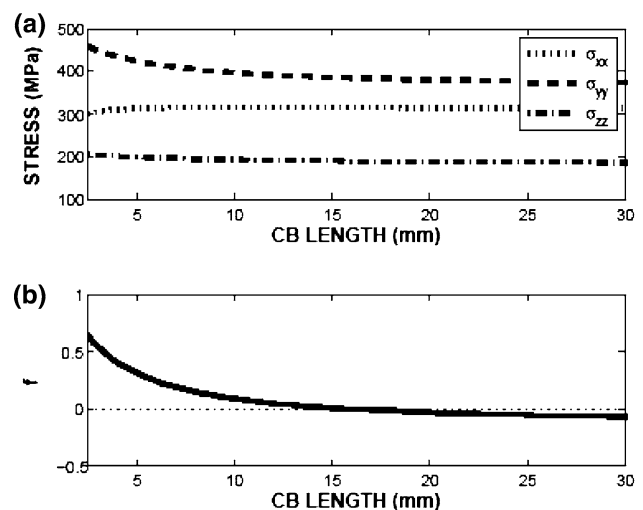


Fig. 6 Prediction of the final length of an un-emptied compaction band developed in Berea Sandstone (BS, Table 1) under specific applied stress conditions. This figure may be compared to Fig. 7 to study the influence of the maximum principal stress, σ_1 , on the length of CB emanating from a borehole (Case 1, see text). The applied principal stresses are $\sigma_1 = 100$ MPa, $\sigma_3 = 40$ MPa, and $\sigma_2 = 50$ MPa. The σ_{xx} , σ_{yy} , and σ_{zz} are the stress components at the tip of a CB emanating from a borehole. f is the yield function for compaction. **a** The σ_{xx} , σ_{yy} , and σ_{zz} stress components are calculated from Eqs. 1–6 and plotted as a function of CB length. **b** The yield function $f(\sigma_{ij})$ is calculated from Eq. 9 using stress components depicted in Fig. 6a and Critical State Model parameters for Berea Sandstone [2] as closest to BS in Quartz content. Once $f(\sigma_{ij})$ drops below zero, CB propagation stops. The predicted CB length is $c = 15.7$ mm

length. Case (3) is an un-emptied CB (as in Fig. 1; Table 3). In Sheets and Haimson [31], (see their Figs. 11c, 12), an un-emptied CB is created using increased drilling-fluid (mud) weight (1.05). This case is compared to Case (4), where an emptied CB (Fig. 2; Table 3) was created by Sheets and Haimson [31]), (their Figs. 8, 9c) under conditions of a very high flow rate (0.06 L/s). In both cases, Mansfield Sandstone (MS) was compressed (Table 1) under far-field loading conditions, with $\sigma_1 = 50$ MPa, $\sigma_3 = 30$ MPa, and $\sigma_2 = 40$ MPa (Table 3). For this calculation x_0 was taken as 1.6 grains ($x_0 = 0.32$ mm, as discussed in the Appendix). The yield function $f(\sigma_{ij})$ is calculated using the Bentheim Sandstone parameters [2], Table 2 here, since it is the rock closest to MS in its Quartz content.

In Case 3, an un-emptied CB, $\sigma_1 = 50$ MPa, $\sigma_3 = 30$ MPa, and $\sigma_2 = 40$ MPa (Table 3; Fig. 8a, b), the procedure for predicting the breakout length is the same as that described for Cases (1) and (2). Under the applied loading, σ_{xx} , σ_{yy} , and σ_{zz} at the tip (Eq. 6) are calculated and plotted (Fig. 8a), then $f(\sigma_{ij})$ (Fig. 8b) is found from (Eq. 9). The theoretically predicted CB length (Fig. 8a) is $c = 3.5$ mm (Table 3). Fig. 12 in Sheets and Haimson [31] gives experimentally measured breakout length also of $c = L - R = 3.5$ mm.

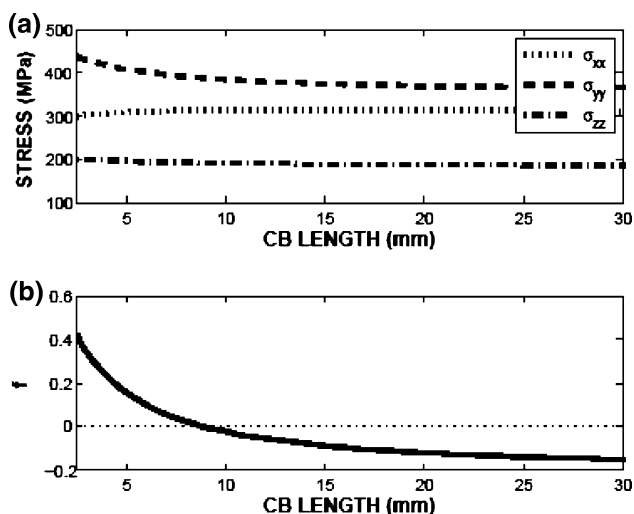


Fig. 7 Prediction of the final length of an un-emptied compaction band developed in Berea Sandstone (BS, Table 1) under specific applied stress conditions. This figure may be compared to Fig. 6 to study the influence of the maximum principal stress, σ_1 , on the length of CB emanating from a borehole (Case 2, see text). The applied principal stresses are $\sigma_1 = 90$ MPa, $\sigma_3 = 40$ MPa, and $\sigma_2 = 50$ MPa. σ_{xx} , σ_{yy} , and σ_{zz} are the stress components at the tip of a CB emanating from a borehole. f is the yield function for compaction. **a** The σ_{xx} , σ_{yy} , and σ_{zz} stress components are calculated from Eqs. 1–6 and plotted as a function of CB length. **b** The yield function $f(\sigma_{ij})$ is calculated from Eq. 9 using stress components depicted in Fig. 7a and Critical State Model parameters (Table 2) for Berea Sandstone [2] as closest to BS in Quartz content. Once $f(\sigma_{ij})$ drops below zero, CB propagation stops. The predicted a CB length is $c = 9.2$ mm

For Case 4, an emptied CB, with $\sigma_1 = 50$ MPa, $\sigma_3 = 30$ MPa, and $\sigma_2 = 40$ MPa (Table 3; Fig. 9a, b), σ_{xx} , σ_{yy} , and σ_{zz} at the breakout tip are calculated from Eqs. 7a, b, and depicted in Fig. 9a. Then $f(\sigma_{ij})$ (Fig. 9b) is found from (Eq. 9). This $f(\sigma_{ij})$ is found to grow infinitely thus predicting that an emptied CB length increases in an unstable manner (Table 3). However, from Fig. 8 in Sheets and Haimson [31], although the experimentally measured CB length is very long, it is finite, with $c = L - R = 35.5$ mm. This discrepancy between the theoretical prediction of the infinite growth of the emptied CB through the sample, and the experimental results showing that the long emptied CB stops growing after reaching a modest length, is analyzed in “Discussion”.

6 Discussion

This work predicts analytically the expected final lengths of compaction bands created around holes, with practical implications to breakouts spontaneously formed in the vicinity of boreholes [13–15, 31]. In particular, two different defect types are studied, both created by localized compaction: the first defect type is a filled compaction band

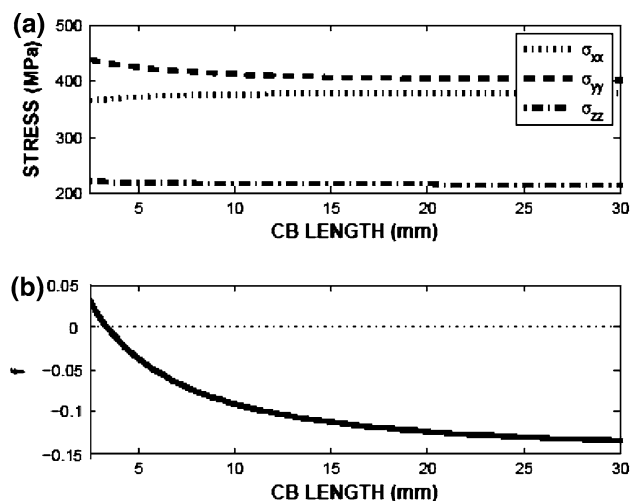


Fig. 8 Prediction of the final length of an un-emptied compaction band developed in Mansfield Sandstone (MS, Table 1) under specific applied stress conditions. This figure may be compared to Fig. 9 to study the extent of CB emptying, on the length of CB emanating from a borehole (Case 3, see text). The applied principal stresses are $\sigma_1 = 50$ MPa, $\sigma_3 = 30$ MPa, and $\sigma_2 = 40$ MPa. σ_{xx} , σ_{yy} , and σ_{zz} are the stress components at the tip of a CB emanating from a borehole. f is the yield function for compaction. **a** The σ_{xx} , σ_{yy} , and σ_{zz} stress components are calculated from Eqs. 1–6 and plotted as a function of CB length. **b** The yield function $f(\sigma_{ij})$ is calculated from Eq. 9 using stress components depicted in Fig. 8a and Critical State Model parameters (Table 2) for Bentheim Sandstone [2] as closest to MS in Quartz content. Once $f(\sigma_{ij})$ drops below zero, CB propagation stops. The predicted a CB length is $c = 3.5$ mm

(CB), and the second is an emptied CB where circulating fluid removes the broken grains that initially formed the CB. The analytical solution that is developed here relies on Katsman et al. [22, 23], who calculated the stress distribution around emptied and un-emptied defects and concluded that the stress fields around these defects are completely different. Therefore it is understandable that the resulting defect elongation, which is dictated by the stress fields, would also be different. We compare our analytical results to the experimental results of Haimson and Kovacich [14] and Sheets and Haimson [31]. The experimental results in [14, 31] point to two main parameters (among others) as affecting final CB length:

1. The value of the applied maximum principal stress (studied systematically only for un-emptied CBs in the present paper);
2. The extent to which the circulating fluid empties the CB.

It can be concluded from the analysis of the results in Cases 1 and 2 that the trend demonstrated by the experiments [14, 31] is preserved: Smaller CB length is obtained under smaller maximum principal stress σ_1 . This conclusion can also be justified by the following arguments: Figs. 6a and 7a demonstrate that at equal σ_3 and σ_2 but

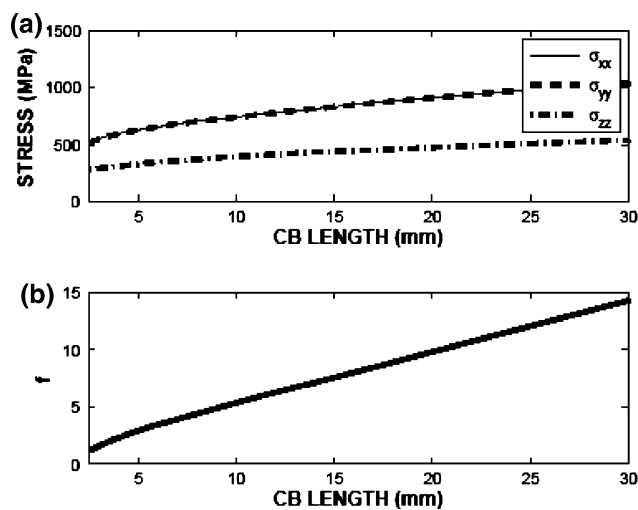


Fig. 9 Prediction of the final length of emptied compaction band developed in Mansfield Sandstone (MS, Table 1) under specific applied stress conditions. This figure may be compared to Fig. 8 to study the extent of CB emptying, on the length of CB emanating from a borehole (Case 4, see text). The applied principal stresses are $\sigma_1 = 50$ MPa, $\sigma_3 = 30$ MPa, and $\sigma_2 = 40$ MPa. σ_{xx} , σ_{yy} , and σ_{zz} are the stress components at the tip of a CB emanating from a borehole. f is the yield function for compaction. **a** The σ_{xx} , σ_{yy} , and σ_{zz} stress components are calculated from Eq. 7a–c and plotted as a function of CB length. **b** The yield function $f(\sigma_{ij})$ is calculated from Eq. 9 using stress components depicted in Fig. 9a and Critical State Model parameters (Table 2) for Bentheim Sandstone [2] as closest to MS in Quartz content. An infinite CB length is predicted as $f(\sigma_{ij})$ does not drops below zero

different σ_1 (Cases 1 and 2), $\sigma_{xx}(\text{tip})$ and $\sigma_{zz}(\text{tip})$ remain almost identical. This is easily demonstrated by expanding $\sigma_{xx}(\text{tip})$, $\sigma_{yy}(\text{tip})$, and $\sigma_{zz}(\text{tip})$ from Eq. 6 (derived from Eqs. 1 and 5) into a Taylor series, assuming $L^2 \gg R^2$ (Fig. 1). To a first order this expansion predicts that $\sigma_{xx}(\text{tip})$ is independent of σ_1 (and also of σ_2 as under constant strain conditions). In the same manner, $\sigma_{yy}(\text{tip})$ is independent of σ_3 and σ_2 , while, $\sigma_{zz}(\text{tip})$ depends only on σ_2 . The resulting $f(\sigma_{ij})$ (Eq. 9) formulated in Cases 1 and 2 has exactly the same form, differing in the value of σ_1 only. This explains why when σ_1 is larger, $f(\sigma_{ij})$ exceeds zero for longer distances away from the CB tip, resulting in longer CBs as in Case 1 relative to Case 2. This analysis is in agreement with results of experiments studying the influence of the maximum principal stress [13, 14, 24].

In comparing the predicted CB length under different extent of emptying (emptied vs. un-emptied), our model demonstrates that at the same applied loading, the final length of emptied CBs is much larger than that of un-emptied CBs (cases 3, 4, Table 3; Figs. 8b, 9b). Equation 7s for the emptied CB predicts that the stresses at the defect tip continue to increase as the emptied CB elongates, as does the resulting $f(\sigma_{ij})$ (Eq. 9), which never falls below zero thus resulting in unbounded growth of an emptied CB.

However, even though in experiments the emptied CB is indeed found to be much longer than the experimentally formed un-emptied CB (Table 3), its length is still finite—i.e., the breakout did not tear through the sample [31]. In our opinion, the reason is that as the breakout reaches some modest length, the injected fluid does not succeed to immediately evacuate all the compacted and loosened grains from the breakout tip. Eventually, a partially emptied CB (point 3 in Sect. 3), characterized by an almost constant stress at its tip, is created, thus reaching a finite length.

In general, unlimited growth of the emptied CBs, which have a stress field that is basically similar to that of cracks, is caused by the fact that such emptied defects do not carry or transmit the applied load (either in compression or in extension), and thus the stress at their tips grows as they elongate [22, 23]. In contrast, localized volume reduction defects, like filled CBs, do carry and transmit the applied load. They are characterized by a constant stress at their tips, and thus by bounded growth and restricted length.

It should be added that the only evidence of empty CBs available now comes from lab tests [4, 14, 31]. Why do not we see these emptied CB's emanating from boreholes in the field? Because logging tools developed so far have no capability to “see” deep enough to identify very narrow slots extending radially from borehole walls.

7 Conclusions

This work aims to explain the results of drilling experiments [13, 14, 24, 31], in which a borehole within porous sandstone is placed under far-field true triaxial compressive stresses, mimicking real in situ conditions. Under certain states of far-field stress and rock strength characteristics, rock failure around the borehole creates breakouts. Breakouts initiate at the borehole wall, at points subjected to the highest compressive stress concentration resulting from the preexisting far-field stress. Based on microscale analysis of tested specimens, it has been inferred that breakouts are preceded by compaction bands. These are induced by the compressive stress concentration across the plane traversing the borehole center and oriented perpendicular to the maximum principal stress. The debonded and often fragmented grains within the compaction band are removed by the circulating drilling fluid, creating the breakout. A new analytical model is developed here in order to study the stress field around these defects and determine factors affecting final breakouts lengths. It is shown that unlimited growth of empty defects, like cracks or emptied CBs, is caused by the fact that these defects do not transmit the applied load under either compression or extension, thus causing the stress at their tips to grow as

they elongate. In contrast, volume reduction defects, such as un-emptied CBs, do carry and transmit the applied load. They are characterized by a constant stress at the vicinity of their tip, independent of their length, thus restricting their growth and their final length. Next, the presence of a borehole also affects the stress field around both types of the defect. Finally, compaction band length increases with increasing applied main principal stress. The model shows remarkable agreement with the experimental results of Haimson and co-workers [13, 14, 24, 31].

8 Appendix: The compactive process zone length x_0

To avoid the stress singularity [30] at the un-emptied/emptied CB tips, one may define the tip stress as the stress at some infinitesimal distance x_0 from the CB tip. A physically motivated choice for x_0 would be a characteristic nucleation length-scale or “compactive process zone” as in Tembe et al. [34]. In light of this definition, compaction nucleation at a CB tip is a process presumably affecting larger rock volumes than the cracking process at a crack tip. The compaction process is accommodated by grain crushing and grain rearrangement. If grain crushing is the dominant mechanism, then a single grain is enough for compaction to occur. Otherwise, if grain rearrangement is the dominant process, then several grains will be involved in the compaction process. The conclusion is that the compactive process zone (in each dimension) may consist of either one or several grains, depending on the dominant physical process, and the local stress components can be applicable to this scale. To approximate the analytically predicted dimensions of the process zone, a contour along which the yield function vanishes ($f(\sigma_{ij}) = 0$) should be drawn around defect tip using Eq. 9 for $f(\sigma_{ij})$ and Eqs. 6 or 7 for the stress field relevant for either un-emptied or emptied CB (this procedure is explained in Tembe et al. [34]). Such a contour is expected to enclose a region of compactive damage in 2D. In our case, un-emptied/emptied CBs emanating from the borehole in both the Berea and Mansfield sandstones studied here were characterized by uniform thickness [14, 31] (see also Sect. 4.1.1). Therefore, we decided to calculate the compactive process zone in 1D only, evaluating the process zone length x_0 along the X axis ($Y = 0$) only using Eq. 9. A trial process zone length x_0 was calculated at several locations as the CB advanced, and the average x_0 was used in all subsequent calculations: $x_0 = 2.2$ mm for BS and $x_0 = 0.32$ mm for MS (see Eqs. 6c, 7c). These values are in good agreement with those of Berea and Bentheim sandstones, found both theoretically and experimentally (from microstructural observations) in Tembe et al. [34].

Furthermore, in the current paper x_0 was calculated at several locations as the CB advanced in each specific case of study. Comparing x_0 in Cases 1 and 3 as the CB advanced demonstrates that when the overall stress field is more intensive, x_0 is larger. The most significant variations in x_0 as the CB advanced were observed in Case 4. Consequently, a separate research may study how process zone length x_0 depends not only on the microstructural properties of the rock [34], but also on the stress distribution around the defect tip.

Acknowledgments The research work of Aharonov and Katsman is supported by grants from the Israel Science Foundation No.732/05 and No.571/08. Haimson’s contribution was supported by the US Office of Basic Energy Sciences, US Department of Energy Grant DE-FG02-98ER14850. We thank both reviewers for their thorough reviews and helpful suggestions.

References

- Baud P, Klein E, Wong T-F (2004) Compaction localization in porous sandstones: spatial evolution of damage and acoustic emission activity. *J Struct Geol* 26(4):603–624
- Baud P, Vajdova V, Wong T-F (2006) Shear-enhanced compaction and strain localization: inelastic deformation and constitutive modeling of four porous sandstones. *J Geophys Res*. doi: 10.1029/2005jb004101
- Brudy M, Zoback MD, Fuchs K, Rummel F, Baumgartner J (1997) Estimation of the complete stress tensor to 8 km depth in the KTB scientific drill holes: implications for crustal strength. *J Geophys Res Solid Earth* 102(B8):18453–18475
- Dresen G, Stanchits S (2008) Borehole breakouts and sand production in porous sandstone. *Geophys Res Abstr*, EGU General Assembly 2008, 10: EGU2008-A-07172
- Eshelby JD (1957) The determination of the elastic field of an ellipsoidal inclusion, and related problems. *Proc R Soc Lond (A)*. *Math Phys Sci* 241(1226):376–396
- Fairhurst C (1968) Methods of determining in situ rock stresses at great depth. Technical report I-86, Missouri River Division, US Army Corps of Engineers
- Germanovich LN, Dyskin AV (2000) Fracture mechanisms and instability of openings in compression. *Int J Rock Mech Mining Sci* 37(1–2):263–284
- Gough DI, Bell JS (1981) Stress orientations from oil-well fractures in Alberta and Texas. *Can J Earth Sci* 18(3):638–645
- Haimson BC (2003) Borehole breakouts in Berea Sandstone reveal a new fracture mechanism. *Pure Appl Geophys* 160:813–831
- Haimson BC (2007) Micromechanisms of borehole instability leading to breakouts in rocks. *Int J Rock Mech Mining Sci* 44(2):157–173
- Haimson BC, Chang CD (2002) True triaxial strength of the KTB amphibolite under borehole wall conditions and its use to estimate the maximum horizontal in situ stress. *J Geophys Res Solid Earth* 107(B10):2257
- Haimson BC, Herrick C (1986) Borehole breakouts—a new tool for estimating in situ stress? In: Stephansson O (ed) *Rock stress*. CENTEK Publishers, Lulea, pp 271–280
- Haimson BC, Klaetsch A (2007) Compaction bands and the formation of slot-shaped breakouts in St. Peter sandstone. *Rock*

- Physics and Geomechanics in the Study of Reservoirs and Repositories 284:89–105
14. Haimson BC, Kovachich J (2003) Borehole instability in high-porosity Berea sandstone and factors affecting dimensions and shape of fracture-like breakouts. *Eng Geol* 69:219–231
 15. Haimson BC, Song I (1993) Laboratory study of borehole breakouts in cordova cream—a case of shear failure-mechanism. *Int J Rock Mech Mining Sci Geomech Abstr* 30(7):1047–1056
 16. Haimson BC, Song I (1998) Borehole breakouts in Berea Sandstone: two porosity-dependent distinct shapes and mechanisms of formation. *Rock Mech Petrol Eng Soc Pet Eng* 1:229–238
 17. Issen KA, Rudnicki JW (2000) Conditions for compaction bands in porous rock. *J Geophys Res* 105(B9):21529–21536
 18. Issen KA, Rudnicki JW (2001) Theory of compaction bands in porous rock. *Phys Chem Earth (A)* 26(1–2):95–100
 19. Jaeger JC, Cook NGW (1976) *Fundamentals of rock mechanics*. Chapman & Hall, London
 20. Katsman R, Aharonov E, Scher H (2005) Numerical simulation of compaction bands in high-porosity sedimentary rock. *Mech Mat* 37(1):143–162
 21. Katsman R, Aharonov E (2006) A study of compaction bands originating from cracks, notches, and compacted defects. *J Struct Geol* 28(3):508–518
 22. Katsman R, Aharonov E, Scher H (2006a) A numerical study on localized volume reduction in elastic media: some insights on the mechanics of anticracks. *J Geophys Res*. doi:10.1029/2004JB003607
 23. Katsman R, Aharonov E, Scher H (2006b) Localized compaction in rocks: Eshelby's inclusion and the Spring Network Model. *Geophys Res Lett* 33(10):L10311
 24. Klaetsch AR, Haimson BC (2002) Porosity-dependent fracture-like breakouts in St. Peter sandstone. In: Hammah R et al. (eds) *Mining and tunneling innovation and opportunity*, University of Toronto press, pp 1365–1371
 25. Klein E, Baud P, Reuschle T, Wong T-f (2001) Mechanical behaviour and failure mode of bentheim sandstone under triaxial compression. *Phys Chem Earth (A)* 26(1–2):21–25
 26. Mollema PN, Antonellini MA (1996) Compaction bands: a structural analog for anti-mode I cracks in aeolian sandstone. *Tectonophysics* 267(1–4):209–228
 27. Murakami Y (1987) *Stress intensity factors handbook*. Soc Mater Sci, Japan
 28. Olsson WA (2001) Quasistatic propagation of compaction fronts in porous rock. *Mech Mater* 33:659–668
 29. Reinecker J, Heidbach O, Tingay M, Sperner B, Müller B (2005) The release 2005 of the World Stress Map. Available at <http://www.world-stress-map.org>
 30. Scholz CH (2000) *The mechanics of earthquakes and faulting*. Cambridge University Press, Cambridge
 31. Sheets RJ, Haimson BC (2004) Drilling variables affecting fracture-like borehole breakout characteristics. In *Gulf rocks 2004*, reviewed CD-Rom Proceedings, paper ARMA/NARMS 04-484
 32. Sih GC (1973) *Handbook of stress–intensity factors: stress-intensity factor solutions and formulas for reference*. Bethlehem, Pa.: Institute of Fracture and Solid Mechanics, Lehigh University
 33. Song I, Haimson BC (1997) Polyaxial strength criteria and their use in estimating in situ stress magnitudes from borehole breakout dimensions. *Intl J Rock Mech Mining Sci* 34(3–4):116
 34. Tembe S, Vajdova V, Wong T-f, Zhu W (2006) Initiation and propagation of strain localization in circumferentially notched samples of two porous sandstones. *J Geophys Res Solid Earth* 111(B2):B02409
 35. Vajdova V, Wong T-f (2003) Incremental propagation of discrete compaction bands: acoustic emission and microstructural observations on circumferentially notched samples of Bentheim. *GRL* 30(14):1775
 36. Vajdova V, Wong T-f, Farell DE, Issen KA, Challa V (2003) Experimental observation and numerical simulation of initiation and propagation of compaction bands in a sandstone. In: *Proceedings ASCE engineering mechanics conference*, Seattle, July 16–18
 37. Vernik L, Zoback MD (1992) Estimation of maximum horizontal principal stress magnitude from stress-induced well bore breakouts in the cajon pass scientific-research borehole. *J Geophys Res Solid Earth* 97(B4):5109–5119